Energy & Environmental Science

Accepted Manuscript

ROYAL SOCIETY OF CHEMISTRY

www.rsc.org/ees

Journal Name

RSCPublishing

COMMUNICATION

Design of a Versatile Interconnecting Layer for Highly Efficient Series-Connected Polymer Tandem Solar Cells

Cite this: DOI: 10.1039/x0xx00000x

Received 00th January 2012,
Accepted 00th January 2012

DOI: 10.1039/x0xx00000x

www.rsc.org/

Lijian Zuo,[a,b] Chih-Yu Chang,[b,c] Chu-Chen Chueh,[b] Shuhua Zhang,[a] Hanying Li,[a] Alex K.-Y. Jen,[a,b*] and Hongzheng Chen [a*]

A versatile interconnecting layer (ICL) based on reflective ultra-thin Ag (8-14 nm) was developed to enable the fabrication of a series-connected micro-cavity tandem polymer solar cell. This novel ICL can manipulate the optical field distribution between the constituent sub-cells to address the challenge of current matching. As a result, a very high power conversion efficiency (~11%) and high summed external quantum efficiency of >90% were demonstrated.

Organic solar cells (OSCs) possess the advantages of low cost, light weight, and good mechanical flexibility, making them attractive for integration into large-area solar arrays to effectively convert sunlight into electricity. Among various types of OSCs that have been reported so far, the series-connected tandem (SCT) structure, in which two or more sub-cells are electrically connected in series by transparent interconnecting layer (ICL), is one of the most promising device structures for efficient light harvesting.[1-10] More recent studies have also revealed that this structure is promising for practical applications.[11-13]

To develop a high-performance SCTOSC, it is very critical to achieve balanced current density in the constituent sub-cells[14-17] and have an efficient ICL to bridge between them.[6,19-22] The current density of sub-cells needs to be balanced in order to minimize energy loss,[15] since photo-current density (J_{ph}) of a SCTOSC device is dominated by the lower value of the constituent sub-cells.[16-17] This problem can be resolved by using complementary absorbing materials in different sub-cells; however, due to rare availability of high-performance low band-gap (LBG) polymers (E_g <1.5 eV), this approach has only seen very limited success so far. Consequently, it remains very challenging to fabricate high efficiency SCTOSC devices. To date, only a few LBG polymers such as poly[2,7-(5,5-bis-(3,7-dimethyl-octyl)-5H-dithieno[3,2-b:20,30-d]pyran)-alt-4,7-(5,6-difluoro-2,1,3-benzothiadiazole)] (PDTP-DFBT) have been used to realize high power conversion efficiency (PCE) SCTOSC devices.[23-25]

In addition to employing materials with complementary absorption, proper optical manipulation can also be used to fine-tune the optical field in the sub-cells to achieve matched J_{ph}.[14,26-27] Recently, Sergeant[28] and Jen[29] have independently demonstrated that an optical micro-cavity can be employed to effectively enhance light trapping in single junction devices to improve their performance. Based on the successful demonstration of optical micro-cavity chambers formed from reflective semi-transparent ultra-thin metal electrodes, it should be feasible to integrate ultra-thin metal films into the SCTOSC architecture to modulate the optical field distribution within the sub-cells. Such films, serving as an ICL, can manipulate the reciprocity in reflection and transmission of incoming light to simultaneously balance J_{ph} of constituent sub-cells and enhance photocurrent generation of resultant tandem devices.

In addition to the function of optical manipulation, an optimal ICL for efficient SCTOSCs needs to possess the following properties:[20-22] 1) it must form an Ohmic contact with the sub-cells for efficient charge collection, 2) it must serve as an efficient electron-hole recombination site, and 3) it must have good optical transparency and solvent resistance. To date, composite films based on poly(3,4-ethylenedioxythiophene):poly(styrenesulfonate) (PEDOT:PSS)/TiO_2[3] are some of the most commonly used ICLs, where PEDOT:PSS serves as the hole-transporting layer (HTL) while TiO_2 functions as the electron-transporting layer (ETL). There are also several other PEDOT:PSS-based ICLs including PEDOT:PSS/ZnO,[1,7] PEDOT:PSS/ZnO/polyelectrolyte,[4] and PEDOT:PSS/polyelectrolyte[5,23], which have been reported to enable SCTOSCs to achieve high PCEs of over 10%.[24-25]

However, PEDOT:PSS-based ICLs have encountered problems with strong acidity[23] and optical loss.[19] To alleviate these problems, alternative ICLs such as MoO_3 have been exploited, which also

afford very high PCEs of over 10%.[31] However, none of these reported ICLs[2,5,32-33] have high enough conductivity to function as an electrode. Although an ICL in the SCTOSC is not required to be highly conductive, higher conductivity enables the sub-cells to work individually, which is beneficial if one wishes to examine the working mechanisms of tandem devices for further optimization.[29-30] Therefore, it is imperative to develop more efficient ICLs to improve the performance of SCTOSCs.

To achieve this goal, we have designed a novel ICL, MoO_3/Ag/poly[(9,9-bis(3-(N,N-dimethylamino)-propyl)-2,7-fluorene)-alt-2,7-(9,9-dioctyl-florene)] (PFN), to realize a high-performance SCTOSC (device structure shown in **Figure 1a**).[34] This ICL comprising MoO_3/Ag/polyelectrolyte can not only facilitate a tailored cascade energy arrangement for efficient electrical connection between the sub-cells, but can also provide effective optical manipulation between them *via* the micro-cavity derived from the embedded ultra-thin Ag (8-14 nm). The reflectivity of the ultrathin metal can manipulate the optical field distribution within the sub-cells (shown in **Figure 1b**). Ideally, most of the high energy photons should be reflected by this ultra-thin Ag layer while the transmitted low energy photons should be effectively confined in the back sub-cell *via* the micro-cavity effects, as demonstrated in our previous work.[35] Given these advantages, proper J_{ph} matching can be achieved within the series-connected tandem cells. As a result, a very high summed external quantum efficiency (EQE) of > 90% and PCE of ~ 11% are successfully demonstrated, where two efficient donor polymers, polyindaceno-dithiophene-alt-quinoxaline (PIDT-PhanQ)[36] and polythieno[3,4-b]thiophene-alt-benzodithiophene (PTB-7)[37] were blended with [6,6]-phenyl-C_{71}-butyric acid methyl ester ($PC_{71}BM$) as the BHJ layers in the front and back sub-cells, respectively (chemical structures are shown in **Figure S1**). In addition, the high conductivity of the Ag-containing ICL layer allows the sub-cells to work separately, facilitating device optimization and study of the working mechanisms of SCT solar cells. Due to efficient light utilization, this tandem architecture has the potential to fully optimize PSC device performance.

In order to effectively collect charges from both sub-cells, the energy level of the ICL should match those of the sub-cells, with one side having a high work function (WF) for collecting holes and the other side having a low work function for collecting electrons. To achieve this arrangement, the WFs of both sides of the ICL (MoO_3/Ag/PFN) were carefully evaluated by using ultra-violet photoelectron (UPS) spectroscopy. As shown in **Figure 2a**, the WF of ITO substrate is measured as ~ 4.60 eV, which is similar to other reports in the literature.[27] The deposited MoO_3 layer shifts the WF energy level (E_f) to 5.31 eV, due to the intrinsically high WF of MoO_3.[30] After depositing another 12-nm-thick Ag film on top of MoO_3, the WF shifts slightly back to 5.08 eV. The further deposition of a 10-nm-thick PFN reduces the WF of the film to 4.29 eV. **Figure S2** shows a schematic diagram of energy levels of the designed tandem architecture with cascade-like energy within the ICL. As a result, this ICL with different WF surfaces can be used to extract both electrons and holes efficiently. Due to the low resistance (< 3.7 Ω/□) of the thin Ag film and the cascade-like energy level within the ICL, efficient recombination of charges extracted from the sub-cells can be expected.

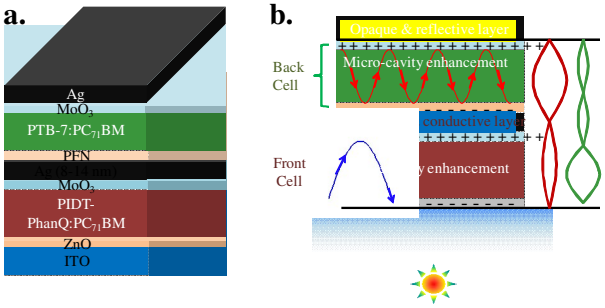

Fig. 1 Schematic diagram of device structure and optical intensity distribution of the series-connected tandem solar cells: **a**. Ultra-thin-Ag-integrated series-connected tandem solar cells with structure of glass/ITO/ZnO/PIDT-PhanQ:$PC_{71}BM$/MoO_3/ultra-thin Ag/PFN/PTB-7:$PC_{71}BM$/MoO_3/Ag. **b**. Schematic illustration of optical field distribution with ultra-thin Ag in ICL: most of the high energy photons are reflected by the intermediate ultra-thin Ag layer, and a micro-cavity effect is formed in the back sub-cell chamber.

Figure S3 shows optical properties of the ultra-thin Ag film (12 nm) on a glass substrate. The transmittance of the ultra-thin Ag film shows a peak at 350 nm (72 %) and then drops sequentially from 350 to 900 nm. The results of optical simulation[30] match well with the experimentally-obtained data, showing that most of the photons are reflected by the ultra-thin Ag layer and optical loss caused by the intrinsic absorption of ultra-thin Ag is very small (< 5 %) in the whole absorbing region.[30] This is consistent with the low absorption coefficient and high reflectivity of Ag film. It has been reported that the deposition of a higher refractive index layer, e.g. TeO_2, could further reduce the reflecting loss in single junction devices.[29] In a SCTOSC, the reflected photons can be re-absorbed by the front cell and converted into photocurrent. Moreover, the transmitted low energy photons can be effectively absorbed by the back sub-cell *via* the micro-cavity effects mentioned above (**Figure 1b**).[29] These results show that the electrical and optical properties of the MoO_3/Ag/PFN ICL are suitable for fabricating SCTOSCs.

Given these advantages, single junction devices with structures similar to those of the sub-cells were fabricated to evaluate the efficacy of the designed ICL and the derived tandem architecture. An inverted device with a configuration of ITO/ZnO/PIDT-PhanQ:$PC_{71}BM$/MoO_3 (10 nm)/Ag (100 nm) (**Figure S4a**), which is similar to that of the front cell shown in **Figure 1a**, was fabricated first. The thickness dependent *J-V* characteristics and EQE spectra are shown in **Figure S4b-4c**. The detailed device performance is summarized in **Table S1**, where the optimal BHJ thickness is determined to be ~ 62 nm. By using an ultra-thin Ag layer (12 nm) as the top electrode, a semi-transparent (ST) device can be obtained accordingly.[38-39] **Figure 2b** shows the corresponding *J-V* characteristics (red line) of the PIDT-PhanQ:$PC_{71}BM$-based ST device, and its detailed device parameters are summarized in **Table S2**. As shown, the

ST device has a PCE of 5.14 %, with similar V_{OC} (0.86 V) and FF (0.66) to those of the control device employing an opaque Ag electrode. Although the J_{SC} of this ST solar cell is much lower than the control device, a considerable amount of light penetrates through to the back sub-cell in the derived tandem device. As shown in **Figure 2c**, this ST device has an averaged ~25 % transmittance in the whole visible region, with a maximum value of ~40 % at 720 nm, suggesting that the PIDT-PhanQ:$PC_{71}BM$ ST device is suitable as the front sub-cell in a SCTOSC.

Next, a device with the configuration glass/Ag/PFN/PTB-7:$PC_{71}BM$/MoO_3/Ag (12 nm)/MoO_3 is fabricated to mimic the back sub-cell. As shown in **Figure 2b** (blue line) and **Table S2**, the sub-cell with the micro-cavity configuration exhibits a PCE of 8.17 % (with a J_{SC} of 15.25 mA/cm^2, a V_{OC} of 0.73 V, and a FF of 0.73), which is comparable to that of an ITO-based counterpart (PCE of 8.22 %) (**Figure S4** and **Table S2**). Due to the high reflectivity of the ultra-thin Ag electrode, a strong micro-cavity effect was formed in the chamber between the ultra-thin Ag layer and the opaque back Ag electrode in this device.[29] Formation of a micro-cavity in such a device structure was also confirmed experimentally, as shown in **Figure S5**. This strong micro-cavity effect results in a significantly enhanced photon-to-electron response centered at 650 nm (**Figure 2d**). Compared to the EQE spectrum of the ITO-based control device (glass/ITO/ZnO/PTB7:$PC_{71}BM$/ MoO_3/Ag), the EQE response of the ultra-thin Ag based device shows higher values from 600-750 nm, which validates the micro-cavity resonant effect that is centered around 700 nm. Also, the 100%-reflection spectrum of the ultra-thin Ag based device (shown in **Figure 2d**) exhibits a similar light-trapping effect beyond 550 nm due to the micro-cavity effect. Note that the 100%-reflection spectrum shows a large discrepancy with the EQE curve from 300 to 500 nm. This is probably due to factors such as absorption from the photo-inactive layer (such as MoO_3 and Ag, etc.), scattering induced by the inhomogeneous ultra-thin Ag layer, and the wavelength-dependent IQE of the device. In addition, the simulated reflectance and active layer absorption shown in **Figure S6** are consistent with our experimental result. The effect of the micro-cavity can also be separately confirmed by optical simulation (**Figure S7**). Notably, the resonant light in the device can be tuned based on the simulated EQE spectra (**Figure S7h**). These results show the potential of using micro-cavities to tune optical field distribution.

The complementary EQE responses between the ultra-thin Ag-based ST device and the micro-cavity device (**Figure 2c-d**) indicate that it is possible to achieve balanced photocurrent for a highly efficient SCTOSC through integration of an ultra-thin Ag film into the ICL of the SCTOSC to modulate optical field distribution within the sub-cells. An ICL formed from such a film can be used to manipulate the reciprocity in reflection and transmission of incoming light simultaneously to achieve balanced J_{SC} between sub-cells and enhance photocurrent generation in resultant tandem devices.

Optical simulations were conducted prior to tandem cell fabrication in order to optimize the device structure and

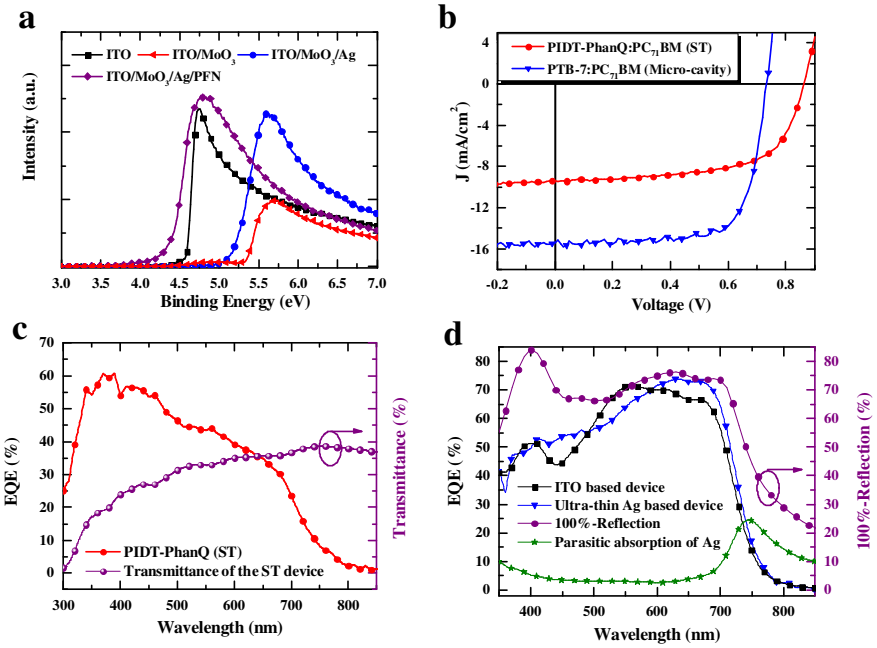

Fig. 2 Properties of ICL (MoO_3/Ag/PFN): **a.** Ultra-violet photoelectron spectroscopy measurement of each layer in the ICL. **b.** *J-V* characteristics of single junction devices. **c.** EQE spectrum of the single junction ST device: glass/ITO/ZnO/PIDT-PhanQ:$PC_{71}BM$/MoO_3/Ag (12 nm) (red line), and its transmittance (purple line). **d.** EQE spectrum of the PTB7-based micro-cavity device: glass/Ag/PFN/PTB7:$PC_{71}BM$/MoO_3/Ag (12 nm)/MoO_3 (blue line), measured 100%-Reflection spectra (purple line), simulated parasitic absorption of top ultra-thin Ag (green line), and EQE spectrum of ITO-based OSC device: glass/ITO/ZnO/PTB7:$PC_{71}BM$/MoO_3/Ag (black line).

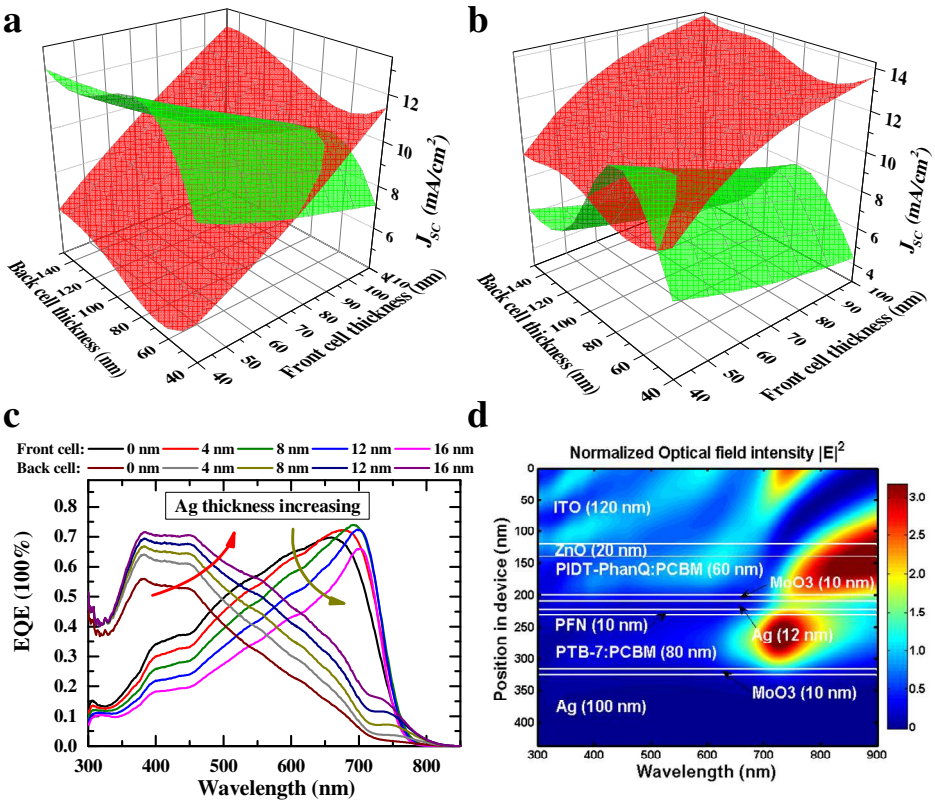

Fig. 3 Optical simulation for tandem devices of glass/ITO/ZnO/PIDT-PhanQ:$PC_{71}BM$ (40-110 nm)/MoO_3/Ag (0 or 12 nm)/PFN/PTB-7:$PC_{71}BM$ (40-150 nm)/MoO_3/Ag). Sub-cell active-layer-thickness-dependent J_{SC} is plotted for the front cell (red surface) and the back cell (green surface): **a.** without Ag in the ICL; **b.** with 12 nm Ag in the ICL. **c.** Ag-thickness-dependent EQE variation of the front and back sub-cells. **d.** The optical distribution in a tandem device with 12 nm Ag in the ICL.

understand optical intensity distribution within the SCTOSC. **Figures 3a-b** and **S8** show how simulated J_{SC} of the sub-cells is affected by sequentially altering the thickness of the Ag layer in the ICL. As shown, if there is no ultra-thin Ag layer, the maximum achievable J_{SC} of SCTOSC (determined by the smaller one of two sub-cells) can only be obtained with a front cell active layer thickness of ~100 nm and a back sub-cell BHJ thickness of ~80 nm. However, when a 12 nm thick Ag layer is inserted in the ICL, the thickness of BHJ in the front cell can be decreased from 100 nm to 60 nm (**Table S3**). It is apparent that the maximum achievable J_{SC} of SCTOSC can be altered by ultra-thin Ag in the ICL when the BHJ layer thickness of the sub-cells is sequentially changed (cross line of red and green surfaces in **Figure 3a-b**). This can be explained by the reflective ultra-thin Ag film increasing the light absorption path in the front sub-cell, resulting in increased J_{SC}. This allows a thinner PIDT-PhanQ:$PC_{71}BM$ BHJ to be used in the front sub-cell while still maintaining high enough FF (**Figure S4**). Consequently, tandem device performance is enhanced. Considering that optimal thickness of the PIDT-PhanQ:$PC_{71}BM$ BHJ is ~ 60 nm as demonstrated previously, the ultra-thin Ag layer provides an effective way to balance current density of the sub-cells to achieve high efficiency. The J_{SC} value of SCTOSC also increases when the ultra-thin Ag layer is inserted in the ICL (**Table S3**) due to the increased light confinement. This result shows that decent reflectivity of the ultra-thin Ag will re-direct the high energy photons into the front sub-cell while effectively confining the transmitted low energy photons in the micro-cavity of the back sub-cell. This will further enhance light utilization.

Further simulations were also conducted to evaluate the J_{SC} in each sub-cell by sequentially changing the thickness of ultra-thin Ag in ICL while fixing the thickness of the BHJ layer of the front and back cells at 60 nm and 80 nm, respectively (**Figure 3c** and **Table 1**). As shown, there are significant deviations of J_{SC} between two sub-cells (front cell: ~6.6 mA/cm^2 and back cell: ~12.1 mA/cm^2) if no ultra-thin Ag layer is included in the ICL. However, J_{SC} of the front cell is significantly increased and that of the back cell gets decreased when increases the Ag thickness. When the thickness reaches 12 nm, a more balanced J_{SC} of the sub-cells can be reached (front sub-cell J_{SC}: 10.64 mA/cm^2, back sub-cell J_{SC}: 10.58 mA/cm^2). This indicates that it is possible to tune current density of individual sub-cells by simply varying the thickness of the Ag layer. Moreover, the summed J_{SC} of two sub-cells, representing the light-trapping properties of the tandem device, increases from 18.6 mA/cm^2 to 21.2 mA/cm^2 when this thin Ag layer is incorporated in the ICL to provide combined reflective and micro-cavity effects. By extracting the ratio of light absorption between two sub-cells, we can calculate the EQE

Table1. Simulated J_{SC} of the sub-cells and the experimental tandem device performance with different thicknesses of Ag in the ICL.

Thickness of Ag layer in ICL	Simulated results			Device performance				
	J_{SC} (front cell)	J_{SC} (back cell)	Summed J_{SC}	J_{SC}	V_{OC}	FF	PCE[a]	
							Average	Best
nm	mA/cm^2	mA/cm^2	mA/cm^2	mA/cm^2	V		%	%
0	6.55	12.08	18.63	5.58	1.28	0.52	3.70	3.82
8	9.21	11.73	20.94	9.20	1.58	0.62	8.74	9.03
10	9.83	11.25	21.08	10.34	1.60	0.64	10.21	10.62
12	10.64	10.58	21.22	9.95	1.60	0.68	10.62	10.98
14	11.14	9.95	21.09	9.09	1.58	0.70	9.78	10.04
16	11.60	9.26	20.86	--	--	--	--	

[a] Over 200 tandem devices were fabricated through ~ 20 batches with a yield of ~ 75%. For the tandem devices with 0, 8, 10, 12, 14 nm Ag in the ICL, 12, 25, 53, 56, and 23 devices are fabricated for average, respectively.

under the assumption of 100% IQE (**Figure S9**). The summed EQE of two sub-cells is over 90% in the whole light absorption range (400-700 nm), which demonstrates the efficacy of the designed tandem architecture for efficient light harvesting.

Figure 3d shows the simulated optical field intensities in the tandem device. When the ultra-thin Ag layer is incorporated into the ICL, most of the high-energy photons (300-600 nm) are localized in the front cell due to enhanced light absorption paths by the reflective metal mirror, and the low-energy (600-780 nm) photons are primarily trapped in the back cell due to the micro-cavity effect. As a result, the optical field intensity in the tandem device is altered and becomes more balanced in the sub-cells.

Based on the results obtained from optimized single junction devices and optical simulations, SCTOSCs with the device structure illustrated in **Figure 1** were fabricated. In this device configuration, thickness of the BHJ layers were fixed at the optimum condition, e.g. ~60 nm for the PIDT-PhanQ:$PC_{71}BM$ based front cell, and ~80 nm for the PTB-7:$PC_{71}BM$ based back cell, to ensure efficient charge transport and collection (**Figure S4**). As mentioned earlier, balanced J_{SC} between sub-cells can be easily achieved by varying the thickness of the ultra-thin Ag layer in the ICL.

As shown **in Figure 4**, without the ultra-thin Ag layer, the tandem device exhibited a PCE of 3.82 %, which is much lower than either one of the optimized single junction devices. In addition, the V_{OC} of the tandem device (1.28 V) is much lower than the summed V_{OC} value of two sub-cells (1.60 V) and a S-shaped *J-V* curve is also observed. This shows the deficiency of using only MoO_3/PFN as the ICL, which causes problems like Schottky barrier at contact, insufficient charge recombination, and charge accumulation, etc. When the ultra-thin Ag layer (8-14 nm) was inserted between MoO_3 and PFN in the ICL, the V_{OC} of the devices increased to nearly the summed value of sub-cells and the *J-V* curves became normal with a FF of over 0.60. This improved performance is due to efficient charge collection/recombination, balanced J_{SC} of the sub-cells, and high conductivity of the ICL. The high-WF MoO_3 forms an Ohmic contact with the front cell to efficiently extract holes to the conductive ultra-thin Ag layer in ICL, as confirmed in the above-mentioned PIDT-PhanQ:$PC_{71}BM$-based single junction device. Vice-versa, the low-WF PFN enables efficient electron extraction. This cascade energy arrangement in the ICL (**Figure S2**) results in efficient electrical connection between sub-cells in the tandem devices.

In order to determine the optimal Ag thickness for the tandem devices, a series of devices with varied Ag thickness (from 8 to 14 nm in ICL) were fabricated. The *J-V* curves of these devices are shown in **Figure S10** and their corresponding performance is summarized in **Table 1**. The J_{SC} of the tandem device reached to the maximum value (10.34 mA/cm^2) when the Ag layer thickness was increased to 10 nm (close to the simulated 12 nm), but dropped afterward. This trend is consistent with the results obtained from optical simulations. When the Ag thickness increases, the J_{SC} of the front cell starts to increase due to the reflection effect, while the J_{SC} of the back cell starts to decrease gradually.

This observation is consistent with the prediction by Forrest[17] that the highest performance of a SCTOSC can be achieved when the J_{MPP} (photo-current at the maximum output power point) rather than the J_{SC} of the sub-cells is most balanced in order to reach good compromise between J_{SC} and FF. This is confirmed by the experimentally measured results from individual sub-cells shown below. Consequently, the best SCTOSC (its *J-V* characteristics is shown in **Figure 4a**) has a PCE of 10.98% (J_{SC} of 9.95 mA/cm^2, V_{OC} of 1.6 V, and FF of 0.68), which represents as one of the highest values reported among double-junction SCTOSCs. The histogram of our tandem solar cell efficiencies is depicted in **Figure S11**, suggesting very good batch-to-batch reproducibility, due to the robust ICL.

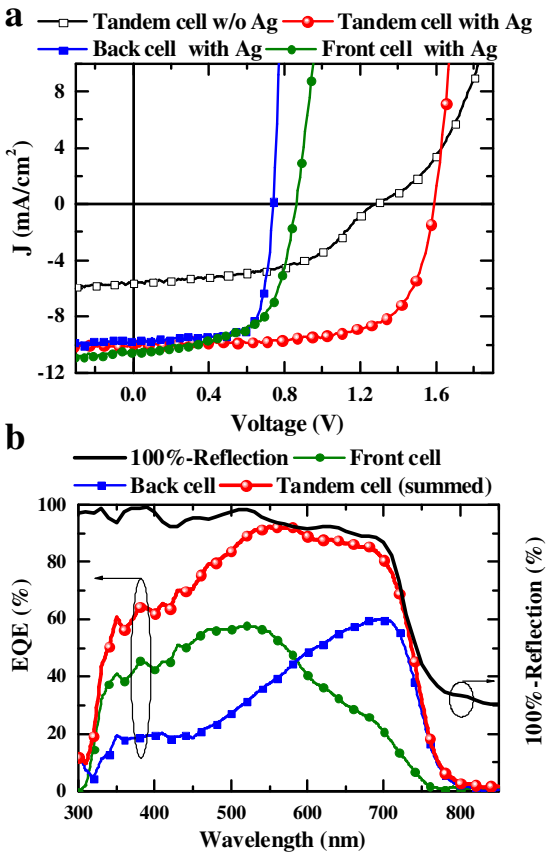

Fig. 4 Tandem solar cell performance (device structure: glass/ITO/ZnO/PIDT-PhanQ:$PC_{71}BM$ (60 nm)/MoO_3 (10 nm)/Ag (0 or 12 nm)/PFP (10 nm)/PTB-7:$PC_{71}BM$ (80 nm)/MoO_3 (10 nm)/Ag (100 nm)): **a.** *J-V* characteristics of the tandem solar cells without (black line) and with (red line) 12 nm Ag in ICL as well as the front cell (green line) and back cell (blue line); **b.** EQE spectrum of the front cell (green line), the back cell (blue line), the summed EQE spectrum of the front and back cells (red line)), and 100%-Reflection spectrum of the tandem device.

Figure 4a shows the *J-V* characteristics of two sub-cells when the highly conductive thin Ag layer is incorporated into the ICL. The back cell possesses a PCE of 5.45 % (with a V_{OC} of 0.74 V, a J_{SC} of 9.76 mA/cm^2, and a high FF of 0.75) and the front sub-cell has a PCE of 5.62 % (with a V_{OC} of 0.86 V, a J_{SC} of 10.41 mA/cm^2, and a FF of 0.63). In spite of the mismatched J_{SC} in these sub-cells, the optimal SCTOSC performance can be obtained due to balanced J_{MPP} of the sub-cells (8.55 and 8.31 mA/cm^2 for front and back sub-cell, respectively). The EQE spectra of the sub-cells and tandem cell with this ICL were also measured individually. As shown in **Figure 4b**, the front cell absorbs most of the high-energy photons (from 330 to 650 nm) and its maximum photo response reaches ~ 57 % at 520 nm when the back cell absorbs most of the low-energy photons (from 500 to 800 nm) reaching its maximum photo response of ~ 58 % at 720 nm, which verifies the previously-discussed micro-cavity effect. The shapes of the EQEs of these sub-cells also resemble those derived from optical simulations (**Figure S6**). It should be noted that the summed EQE of the sub-cells reaches a peak response of 92%, which is the highest value reported in literature. In the plot of 100%-reflection, the highest value can even approach 100% for the tandem device, which validates our experimental EQE curves. This demonstrates the efficacy of the designed tandem device architecture in fully utilizing solar irradiation to improve device performance.

Conclusions

In summary, highly efficient series-connected polymer tandem solar cells were demonstrated by employing a versatile ICL (MoO_3/ultra-thin Ag/PFN) to achieve efficient charge extraction and recombination. The distribution of optical intensity can be optimized through strong reflectivity generated by the ultra-thin Ag layer in ICL to achieve balanced current densities between two sub-cells. This thin reflecting mirror also allows light to be better confined in the tandem structure due to the formation of a micro-cavity in the back sub-cell. A very high PCE of ~11 % could be achieved with a maximum summed EQE peak value exceeding 90 %. In addition, this versatile ICL allows direct measurement of individual sub-cell parameters, improving understanding of the working mechanisms of the tandem cells and encouraging further optimization of their performance.

Acknowledgements

This work was supported by the Major State Basic Research Development Program (2014CB643503), the National Natural Science Foundation of China (Grants 91233114, 51261130582, and 51473142), the Asian Office of Aerospace R&D (FA2386-11-1-4072), and the Office of Naval Research (N00014-14-0170).

Notes and references

[a]State Key Laboratory of Silicon Materials, MOE Key Laboratory of Macromolecular Synthesis and Functionalization, Department of Polymer Science & Engineering, Zhejiang University, Hangzhou 310027, China E-mail: hzchen@zju.edu.cn or ajen@uw.edu
[b]Department of Materials Science and Engineering, University of Washington, Seattle, Washington 98195, USA.
[c]Department of Materials Science and Engineering, Feng Chia University, Taichung, Taiwan

†Electronic Supplementary Information (ESI) available: [Materials and equipment, device fabrication and characterization, and optical simulation]. See DOI: 10.1039/c000000x/

1. L. Dou, J. You, J. Yang, C. C. Chen, Y. J. He, S. Murase, T. Moriarty, K. Emery, G. Li, Y. Yang, *Nat. Photon.* 2012, **6**, 180.
2. J. You, L. Dou, Z. Hong, G. Li, Y. Yang, *Prog. Pol. Sci.* 2013, **38**, 1909.
3. J. Y. Kim, K. Lee, N. E. Coates, D. Moses, T. Q. Nguyen, M. Dante, A. J. Heeger, *Science* 2007, **317**, 222.
4. J. Jo, J. R. Pouliot, D. Wynands, S. D. Collins, J. Y. Kim, T. L. Nguyen, H. Y. Woo, Y. Sun, M. Leclerc, A. J. Heeger, *Adv. Mater.* 2013**, 25**, 4783.
5. Y. Zhou, C. Fuentes-Hernandez, J. W. Shim, T. M. Khan, B. Kippelen, *Energ. Environ. Sci.* 2012, **5**, 9827.
6. N. Li, D. Baran, K. Forberich, M. Turbiez, T. Ameri, F. C. Krebs, C. J. Brabec, *Adv. Energ. Mater.* 2013, **3**, 1597.
7. W. Li, A. Furlan, K. H. Hendriks, M. M. Wienk, R. A. J. Janssen, *J. Am. Chem. Soc.* 2013, **135**, 5529.
8. V. S. Gevaerts, A. Furlan, M. M. Wienk, M. Turbiez, R. A. J. Janssen, *Adv. Mater.* 2012, **24**, 2130.
9. S. Kouijzer, S. Esiner, C. H. Frijters, M. Turbiez, M. M. Wienk, R. A. J. Janssen *Adv. Energ. Mater.* 2012, **2**, 945.
10. H. Zhou, Y. Zhang, C.-K. Mai, S. D. Collins, G. C. Bazan, T.-Q. Nguyen and A. J. Heeger, *Adv. Mater.*, 2015, **27**, 1767.
11. T. R. Andersen, H. F. Dam, M. Hosel, M. Helgesen, J. E. Carle, T. T. Larsen-Olsen, S. A. Gevorgyan, J. W. Andreasen, J. Adams, N. Li, F. Machui, G. D. Spyropoulos, T. Ameri, N. Lemaitre, M. Legros, A. Scheel, D. Gaiser, K. Kreul, S. Berny, O. R. Lozman, S. Nordman, M. Valimaki, M. Vilkman, R. R. Sondergaard, M. Jorgensen, C. J. Brabec and F. C. Krebs, *Energy & Environmental Science*, 2014, **7**, 2925.
12. F. Machui, M. Hosel, N. Li, G. D. Spyropoulos, T. Ameri, R. R. Sondergaard, M. Jorgensen, A. Scheel, D. Gaiser, K. Kreul, D. Lenssen, M. Legros, N. Lemaitre, M. Vilkman, M. Valimaki, S. Nordman, C. J. Brabec and F. C. Krebs, *Energy & Environmental Science*, 2014, **7**, 2792.
13. N. Espinosa and F. C. Krebs, *Solar Energy Materials and Solar Cells*, 2014, **120,** 692.
14. Y. Jin, J. Feng, M. Xu, X. L. Zhang, L. Wang, Q. D. Chen, H. Y. Wang, H. B. Sun, *Adv. Opt. Mater.* 2013, **1**, 809.
15. J. Gilot, M. M. Wienk, R. A. J. Janssen, *Adv. Mater.* 2010, **22**, E67.
16. A. Hadipour, B. de Boer, P. W. M. Blom, *Org. Electron.* 2008, **9**, 617.
17. B. E. Lassiter, C. Kyle Renshaw, S. R. Forrest, *J. Appl. Phys.* 2013, **113**, 214505.
18. M. Hiramoto, M. Suezaki, M. Yokoyama, *Chem.Lett,* 2006, **19**, 327.
19 C. H. Chou, W. L. Kwan, Z. Hong, L. M. Chen, Y. Yang, *Adv. Mater.* 2011, **23,** 1282.
20. J. Yang, R. Zhu, Z. Hong, Y. He, A. Kumar, Y. F. Li, Y. Yang, *Adv. Mater.* 2011, **23**, 3465.
21. Y. Yuan, J. Huang, G. Li, *Green* 2011, **1**, 65.
22. C. C. Chueh, C. Z. Li, A. K. Y. Jen, *Energy & Environmental Science*, 2015, **8**, 1160.
23. Y. Liu, C. C. Chen, Z. Hong, J. Gao, Y. Yang, H. Zhou, L. Dou, G. Li, Y. Yang, *Sci. Rep.* 2013, **3**, 3356.
24. J. You, C. C. Chen, Z. Hong, K. Yoshimura, K. Ohya, R. Xu, S. Ye, J. Gao, G. Li, Y. Yang, *Adv. Mater.* 2013, **25**, 3973.
25. J. You, L. Dou, K. Yoshimura, T. Kato, K. Ohya, T. Moriarty, K. Emery, C. C. Chen, J. Gao, G. Li, Y. Yang, *Nat. Commun.* 2013, **4**, 1446.
26. J. Yang, J. You, C. C. Chen, W. C. Hsu, H. R. Tan, X. W. Zhang, Z. Hong, Y. Yang, *ACS Nano* 2011, **5**, 6210.
27. J. D. Myers, W. Cao, V. Cassidy, S. H. Eom, R. Zhou, L. Yang, W. You, J. Xue, *Energ. Environ. Sci.* 2012, **5**, 6900.
28. N. P. Sergeant, A. Hadipour, B. Niesen, D. Cheyns, P. Heremans, P. Peumans, B. P. Rand, *Adv. Mater.* 2012, **24**, 728.
29. (a) J. F. Salinas, H. L. Yip, C. C. Chueh, C. Z. Li, J. L. Maldonado, A. K. Y. Jen, *Adv. Mater.* 2012, **24**, 6362; (b) K. S. Chen, H. L. Yip, J. F. Salinas, Y. X. Xu, C. C. Chueh, A. K. Y. Jen, *Adv. Mater.* 2014, **26**, 3349; (c) K. Yao, X. K. Xin, C. C. Chueh, K. S. Chen, Y. X. Xu, *Adv. Funct. Mater.* 2015, **25**, 567.
30. G. F. Burkhard, E. T. Hoke, M. D. McGehee, *Adv. Mater.* 2010, **22**, 3293.
31. Z. Zheng, S. Zhang, M. Zhang, K. Zhao, L. Ye, Y. Chen, B. Yang, J. Hou, *Adv. Mater.* 2015, **27**, 1189.
32. T. Ameri, N. Li, C. J. Brabec, *Energ. Environ. Sci.* 2013, **6**, 2390.
33. H. Kang, S. Kee, K. Yu, J. Lee, G. Kim, J. Kim, J. R. Kim, J. K, K. H. Lee, *Adv. Mater.* 2015, **27**, 1408.
34. Z. He, C. Zhong, S. Su, M. Xu, H. B. Wu, Y. Cao, *Nat. Photon.* 2012, **6**, 591.
35. L. J. Zuo, C. C. Chueh, Y. X. Xu, K. S. Chen, Y. Zang, C. Z. Li, H. Z. Chen, A. K. Y. Jen, *Adv. Mater.* 2014, **26**, 6778.
36. Y. Zhang, J. Zou, H. L. Yip, K. S. Chen, D. F. Zeigler, Y. Sun, A. K. Y. Jen, *Chem. Mater.* 2011, **23,** 2289.
37. Y. Liang, Z. Xu, J. Xia, S. T. Tsai, Y. Wu, G. Li, C. Ray, L. Yu, *Adv. Mater.* 2010, **22**, E135.
38. C. C. Chueh, S. C. Chien, H. L. Yip, J. F. Salinas, C. Z. Li, K. S. Chen, F. C. Chen, W. C. Chen, A. K. Y. Jen, *Adv. Energy Mater.* 2013**, 3**, 417.
39. C.Y. Chang, L. Zuo, H. L. Yip, C. Z. Li, Y. X. Li, C. S. Hsu, Y. J. Cheng, H. Z. Chen, A. K. Y. Jen, *Adv. Energy Mater.* 2014**, 4**, 1301645.